

Seismic Inversion After Depth Migration

Maxim Protasov(✉) and Danil Dmitrachkov

Institute of Petroleum Geology and Geophysics, Novosibirsk 630090, Russia
protasovmi@ipgg.sbras.ru, d.dmitrachkov@g.nsu.ru

Abstract. Seismic inversion is used in practice as a tool for predicting reservoir properties. It allows one to extract a model with a high level of detail from seismic data, i.e. high-frequency component of the model. In this case, the input data are the time processing results, and the issues related to the low-frequency component of the model are not considered usually. This work describes the implementation of a model-based seismic inversion algorithm. The input data for the inversion are the depth image results in true amplitudes and the depth migration velocity model. The possibilities of seismic inversion are numerically investigated to refine the low-frequency component of the model. Experiments were carried out using synthetic seismic data got for realistic Sigsbee model.

Keywords: Seismic inversion · Depth migration · Low-frequency model

1 Introduction

Seismic inversion has become a standard procedure, which most times is mandatory for predicting reservoir properties. Traditionally, people consider seismic inversion as an algorithm that provides conversion of a time or migrated time seismic section into an acoustic impedance section [1, 2]. Usually, the input data for inversion result from time processing of seismic data, both pre-stack and post-stack [3, 4].

However, depth processing is often necessary, and seismic inversion is desirable based on the results of the depth processing. There are approaches to perform seismic inversion directly in the depth domain after migration [5], but they are computationally expensive. A simpler approach, when the image after depth migration is transformed into the time domain and standard inversion algorithms based on one-dimensional convolutional modeling, gives reasonable results, and it is this one that is used in practice.

The major result of the standard use of seismic inversion is a detailed model of the elastic properties of the geological environment, which makes it possible to predict the properties of reservoirs [6]. The inversion provides restoring the high-frequency component of the model. However, the low-frequency component "remains in the shadows", although the logic of the inversion operation points out that this part of the model should also be refined. If this is the case, then depth-processing inversion can refine the low-frequency component of the model.

© The Author(s), under exclusive license to Springer Nature Switzerland AG 2022
O. Gervasi et al. (Eds.): ICCSA 2022, LNCS 13375, pp. 173–183, 2022.
https://doi.org/10.1007/978-3-031-10522-7_13

Therefore, within the framework of this work, we investigate seismic inversion in order to determine its capabilities for reconstructing the low-frequency component of the model. We implement model-based seismic inversion algorithm, where we use the migration model as the initial approximation. We provide the study using synthetic data and the Sigsbee model. This paper is organized as follows. First, we present model based seismic inversion, next, we describe briefly the procedure for seismic depth imaging. Then we provide numerical experiments, and we finalize with the conclusion.

2 Model Based Seismic Inversion

Acoustic seismic inversion is based on a one-dimensional convolutional model [2, 3, 7]:

$$S(t) = w(t) * R(t). \tag{1}$$

Here $S(t)$ – seismic trace, $R(t)$ – reflection coefficients, $w(t)$ – seismic impulse. When discretized, Eq. (1) takes the following form:

$$S = \begin{bmatrix} S_1 \\ S_2 \\ \vdots \\ S_N \end{bmatrix} = \begin{bmatrix} w_1 & 0 & 0 & \\ w_2 & w_1 & 0 & \cdots \\ w_3 & w_2 & w_1 & \\ & \vdots & & \ddots \end{bmatrix} \cdot \begin{bmatrix} R_1 \\ R_2 \\ \vdots \\ R_N \end{bmatrix} = WR. \tag{2}$$

Here W – convolution matrix, w_i, S_i,R_i –discrete values of momentum, trace and reflection coefficients, respectively. The model-based inversion algorithm uses a low-contrast approximation [3, 4, 7]:

$$R_i \approx \frac{1}{2}(\ln Z_{i+1} - \ln Z_i). \tag{3}$$

Here Z_i – acoustic impedance. In matrix form, expression (3) looks like this:

$$R = \frac{1}{2}Dx - \frac{1}{2}\widehat{L}. \tag{4}$$

D – N- dimensional matrix, a x, $\widehat{L}$ – N- dimensional vectors:

$$D = \begin{bmatrix} 1 & 0 & 0 & & 0 & 0 \\ -1 & 1 & 0 & \cdots & 0 & 0 \\ 0 & -1 & 1 & & 0 & 0 \\ & \vdots & & \ddots & \vdots & \\ 0 & 0 & 0 & & 1 & 0 \\ 0 & 0 & 0 & \cdots & -1 & 1 \end{bmatrix}, \; x = \begin{bmatrix} \ln Z_2 \\ \ln Z_3 \\ \vdots \\ \ln Z_{N+1} \end{bmatrix}, \; \hat{L} = \begin{bmatrix} \ln \hat{Z}_1 \\ 0 \\ \vdots \\ 0 \end{bmatrix}. \tag{5}$$

We assume in the upper layer the acoustic impedance $\widehat{Z}_1$ to be known. Let us write the system of Eqs. (2) with respect to the vector x (the logarithm of acoustic impedances), substituting expression (4) for the reflection coefficients into it:

$$\frac{1}{2}WDx = S + \frac{1}{2}W\widehat{L}. \tag{6}$$

Then we introduce definitions:

$$C = \frac{1}{2}WD, A = C^T C, b = C^T\left(S + \frac{1}{2}W\widehat{L}\right). \tag{7}$$

Multiplying both parts of the system of Eqs. (6) by the matrix C^T, we arrive at a system of linear algebraic equations (SLAE):

$$Ax = b. \tag{8}$$

The matrices W and D are $N \times N$ square and nonsingular, therefore the matrix $A = C^T C$ is symmetric and positive definite. Therefore, we solve the system (8) by using the conjugate gradient method. To do this, we need an initial approximation - an a priori model of acoustic impedances. Hence the name of this type of inversion, i.e. model-based inversion when it needs some initial model. In the practice, when solving geological problems by seismic inversion, the interpolation of smoothed logging data along the traced horizons provides the initial model.

There is noise in the observed data, and in order to suppress its influence and get an adequate solution, we use regularization. One of the popular approaches is the Tikhonov regularization [8, 9]. It means to move from solving SLAE (8) to the problem of minimizing the parametric functional:

$$\Psi(x, \alpha) = \|Ax - b\|_2^2 + \alpha\|x\|_2^2. \tag{9}$$

Here $\alpha > 0$ and is called the regularization parameter. Too small values of the regularization parameter lead to the original ill-posed problem, and too large values give solutions that have little in common with the original system. Therefore, the choice of the regularization parameter is critically important. One of the most popular approaches for automatic selection of the regularization parameter is the residual principle [10]. It boils down to the fact that, for a noise level ε, the regularization parameter α is the solution of the equation:

$$\|Ax_\alpha - b\|_2 = \|\varepsilon\|_2. \tag{10}$$

This establishes an explicit relationship between the regularization parameter and the errors in the observed data. The efficiency of the method depends on the accuracy of noise estimation. For a seismic inversion problem, this information is usually got from well data.

In order to obtain smooth solutions, the regularization method needs to be changed. To do this, the functional of the form is minimized:

$$\Psi(x, \alpha) = \|Ax - b\|_2^2 + \alpha \|x - x_0\|_2^2. \tag{11}$$

The form of the second term imposes on the solution the requirement of proximity to the initial approximation x_0. Further, it is required that the solution be smooth. We do this using the second-order gradient [8, 11], which in matrix form has the form:

$$D = \begin{bmatrix} -1 & 1 & 0 & \cdots & \cdots & 0 \\ -1 & 2 & -1 & 0 & \cdots & 0 \\ 0 & -1 & 2 & -1 & \ddots & 0 \\ \vdots & \ddots & \ddots & \ddots & \ddots & \cdots \\ \vdots & 0 & 0 & -1 & 2 & -1 \\ 0 & \cdots & \cdots & 0 & -1 & 1 \end{bmatrix}. \tag{12}$$

Then the problem comes to minimizing the functional of the form:

$$\Phi(x, \alpha) = \|Ax - b\|_2^2 + \alpha \|D(x - x_0)\|_2^2. \tag{13}$$

In the work, we implement and use two regularization methods described above. To distinguish between them, the first method, corresponding to the minimization of the functional (11), is conditionally called the "standard" regularization, and the second method, corresponding to the minimization of the functional (13), is called the "maximum smoothness" regularization.

3 Seismic Imaging

For seismic image construction, the Gaussian beam based true amplitude imaging is used [12, 13]:

$$I(\bar{x}; \alpha, \beta) = \int T_p^s(x_s; \bar{x}; \alpha, \beta; \omega) \cdot T_p^r(x_r; \bar{x}; \alpha, \beta; \omega) \cdot d(x_r; x_s; \omega) dx_r dx_s d\omega d\alpha. \tag{14}$$

Here $\boldsymbol{d}$ is the seismic data, $\boldsymbol{x_r}/\boldsymbol{x_s}$ is the source/receiver coordinate, $\boldsymbol{\omega}$ is the frequency, $\boldsymbol{\alpha}, \boldsymbol{\beta}$ are the dip and opening angles, $\boldsymbol{T_p^{s(r)}}$ are the source (receiver) Gaussian beam stacking weights.

This procedure allows one to build images of target objects with high resolution and signal-to-noise ratio. Tracing Gaussian beams from the image points to the observation system is used to achieve such results. We choose beams as the most narrowly focused at the image points. Also, we choose identical Gaussian beams at the image points. Therefore, we provide the uniformity of the resolution throughout the imaging area. However, these Gaussian beams are different depending on the depth and angles on the observation surface. We achieve the maximum image resolution because of the minimization of the Gaussian beam width at the image points. Such a Gaussian imaging algorithm selects coherent events. It focuses the energy on the image point, and therefore it provides Gaussian beam images with high resolution and signal-to-noise ratio.

4 Numerical Examples

To test the developed inversion algorithm, we create a model identical to the one presented in [7]. Then, we calculate the ideal seismic trace by convolving the corresponding model reflection coefficients and the seismic wavelet according to (1). Here, we use a Ricker pulse with a dominant frequency of 20 Hz. Next, we apply seismic inversion using data without noise, but we change the regularization parameter. The results show that as the parameter α increases; the solution becomes smoother (Fig. 1a, 1b). We carried the next series of calculations out for data with the Gaussian noise. The residual principle provides the regularization parameter automatically in this case (Fig. 1c). We note that in the specific case, when the noise level is 15%, the result (Fig. 1c) visually does not differ from the result of similar calculations presented in [7]. The repeatability of the result on identical data shows that the developed algorithms work correctly.

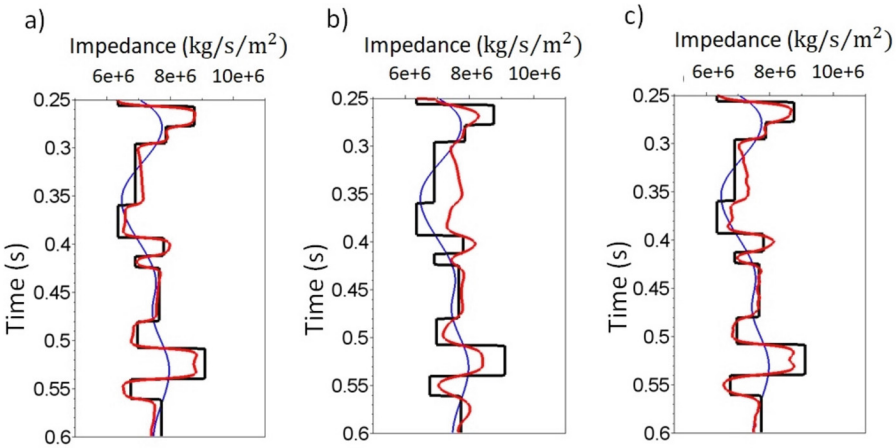

Fig. 1. The result of the model based seismic inversion. Black - true impedances, blue - initial model, red - inversion result: a) data without noise, "standard" regularization parameter $\alpha = 1$; b) data without noise, $\alpha = 20$; c) data with a noise of 15%, with the selection of a parameter according to the residual principle $\alpha = 2.71$. (Color figure online)

In the next series of numerical experiments, we apply the developed model based seismic inversion algorithm to the results of depth seismic migration in true amplitudes. Since both the migration velocity model and the migration result are specified on a depth scale, and seismic inversion works on a time scale, we use the depth-to-time transform [14]. For its implementation, we use migration velocity model. Thus, through this transformation, we get the original and migration Sigsbee models in a time scale and further converted into acoustic impedance values (Fig. 2).

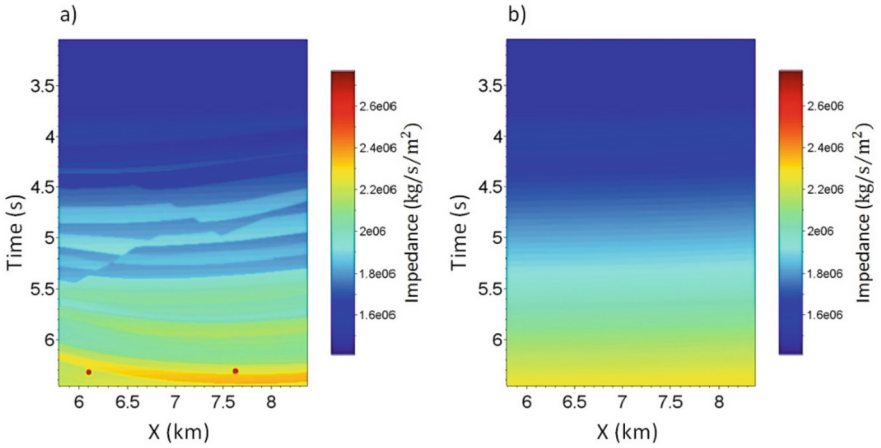

Fig. 2. a) A fragment of the original Sigsbee model (acoustic impedance) converted to time scale. b) Corresponding fragment of the Sigsbee migration model in time scale.

We get the seismic image or seismic traces at the depth scale by using the true amplitude depth migration algorithm described in [12, 13]. Also, in parallel, we construct ideal seismic images, which get when the migration algorithm works correctly and does not contain any artifacts and approximation errors. Formally, such ideal traces result from a two-dimensional convolution of a depth reflection coefficient model with a seismic wavelet [13]. We convert ideal images and depth migration results got in the depth domain to the time scale.

First, we consider one seismic trace after migration for a detailed numerical study (Fig. 3a). One can see that it coincides with the ideal mostly, but there are also discrepancies. We apply the developed seismic inversion algorithm to both traces (Fig. 3b, 3c). Also, we perform calculations for several values of the regularization parameter in order to observe its influence (Fig. 4a, 4b). One can observe that the inversion along the ideal path gives a result that coincides with the true solution with high accuracy (Fig. 3b). However, the result of the inversion of the seismic trace after migration is less accurate, which is a consequence of the difference between the migrated trace and the ideal one (Fig. 3c). One can see that the reconstructed impedance model "captures" many jumps in true impedances, and inaccuracies appear mainly inside the reservoirs. This behavior is partly because of regularization. With an increase in the "standard" regularization parameter, the inversion result is closer to the initial model (Fig. 4a, 4b). One can observe that the "standard" regularization parameter makes it possible to balance between a more accurate description of abrupt changes in the model and more correct values within the layers. To improve this situation, we change the regularization in the inversion. The algorithm uses the "maximum smoothness" regularization (Fig. 4c). One can see that this solution describes the true impedances more accurately than the solution constructed using the "standard" regularization.

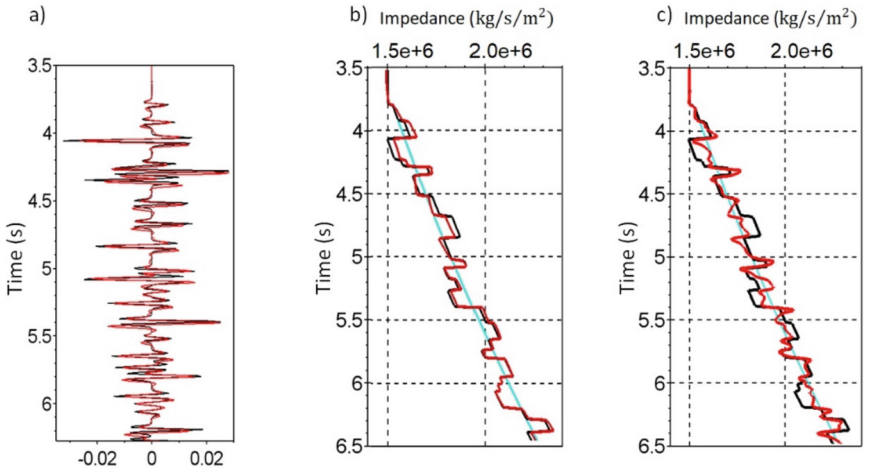

Fig. 3. a) Ideal seismic trace – black, seismic trace after running the migration algorithm – red, x = 6705 m. b) and c) Inversion results of the ideal seismic trace and the seismic trace after migration, respectively, x = 6705 m. Black – true acoustic impedances, turquoise – initial background model, red – inversion result at $\alpha = 0.01$ with "standard" regularization. (Color figure online)

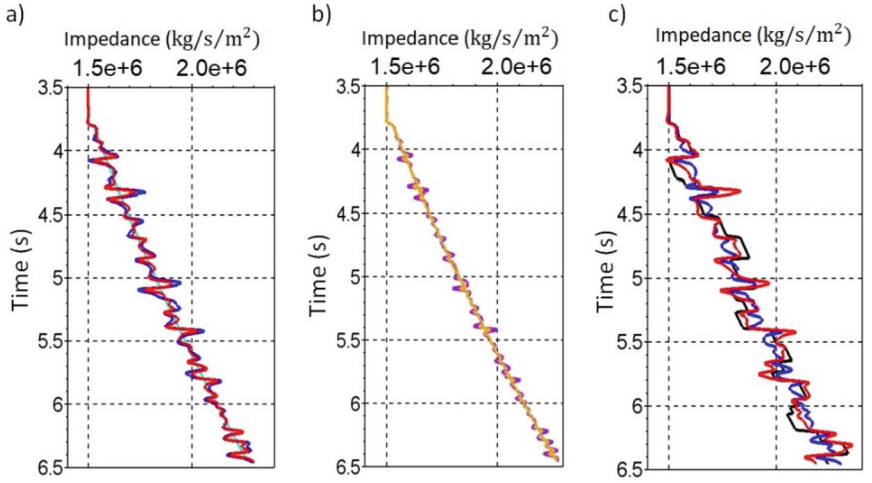

Fig. 4. Seismic inversion results after migration, x = 6705 m. a) Inversion result with "standard" regularization at $\alpha = 0.001$ - blue, at $\alpha = 0.01$ - red, initial model – turquoise. b) The inversion result with "standard" regularization at $\alpha = 0.1$ - violet, at $\alpha = 1.0$ - orange, initial model – turquoise. c) The inversion result with "standard" regularization at $\alpha = 0.01$ - blue, the inversion result with "maximum smoothness" regularization at $\alpha = 0.01$ - red, true acoustic impedances - black. (Color figure online)

Next, we apply seismic inversion to the entire studied fragment of the Sigsbee model using the "maximum smoothness" regularization (Fig. 5). The inversion result shows a satisfactory accuracy of restoring the detailed impedance model in most of it, except the vicinity of diffraction objects and zones containing migration artifacts.

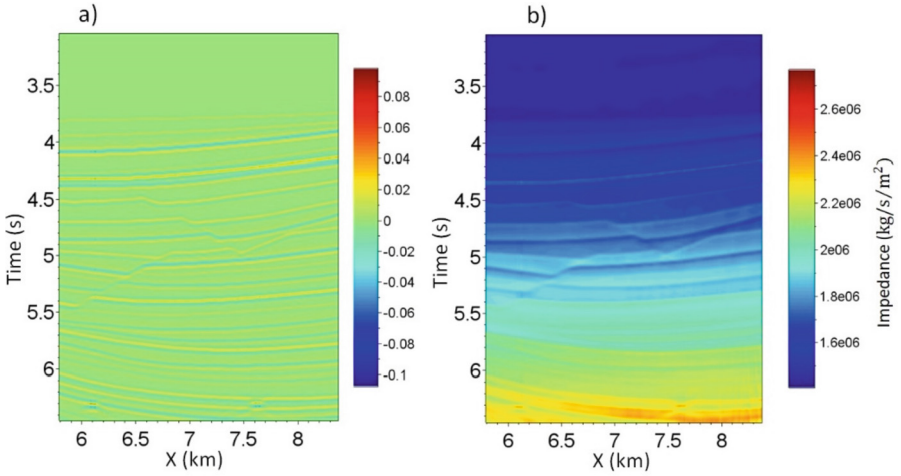

Fig. 5. a) The result of seismic depth migration converted to a time scale. b) Corresponding result of seismic inversion.

The inversion results got above (Fig. 5) show that the seismic inversion of the depth migration results gives a satisfactory result of restoring a detailed model of the environment, including its high-frequency component. One can see that this result describes the seismic model, including the low-frequency component. Of course, the initial model contains part of the low-frequency component, which is used both in inversion and migration, but it is being refined.

To reveal this more clearly, we propose to highlight the low-frequency component of the model by smoothing the inversion result. Here, we apply the same procedure to the true model. We use function with a Gaussian kernel as a smoothing operator:

$$\tilde{y}_i = \frac{\sum_{j=1}^{n} K\left(\frac{x_i - x_j}{b}\right) \cdot y_j}{\sum_{j=1}^{n} K\left(\frac{x_i - x_j}{b}\right)}, \qquad K(t) = \frac{1}{\sqrt{2\pi}(0.37)} e^{-\frac{t^2}{2\cdot(0.37)^2}}. \tag{15}$$

Here x_i – these are the nodes of the grid, and y_i and $\tilde{y}_i$ are the values of the original and smoothed functions on this grid, b is the parameter that controls the smoothness of the resulting function. Next, we provide various low-frequency components of the true model and the result of the inversion by smoothing with different values of the parameter b

(Fig. 6). For large values of b, for example $b = 0.8$, the result of smoothing the true model becomes close to the initial inversion model (Fig. 6a). For small values of b, for example $b = 0.05$, the smoothing result differs little from the true model (Fig. 6a). However, between these values, for example $b = 0.3$, rather smooth solutions are obtained, which differ markedly from the initial model for inversion (Fig. 6a). One can get similar results when smoothing the model got by seismic inversion (Fig. 6b). Comparison of the low-frequency components of the true model, the result of the inversion of "ideal traces" and the traces after migration shows that the inversion determines these components with high accuracy (Fig. 7). Relative root-mean-square error of the trace inversion result after migration (Fig. 8) relative to the true model for the components obtained by smoothing using the parameter $b = 0.3$, equals to 1.35%. When using the parameter $b = 0.1$, the error is 1.78%. Based on these results, we can conclude that the inversion really determines the low-frequency component of the model, while restoring it with a fairly high accuracy.

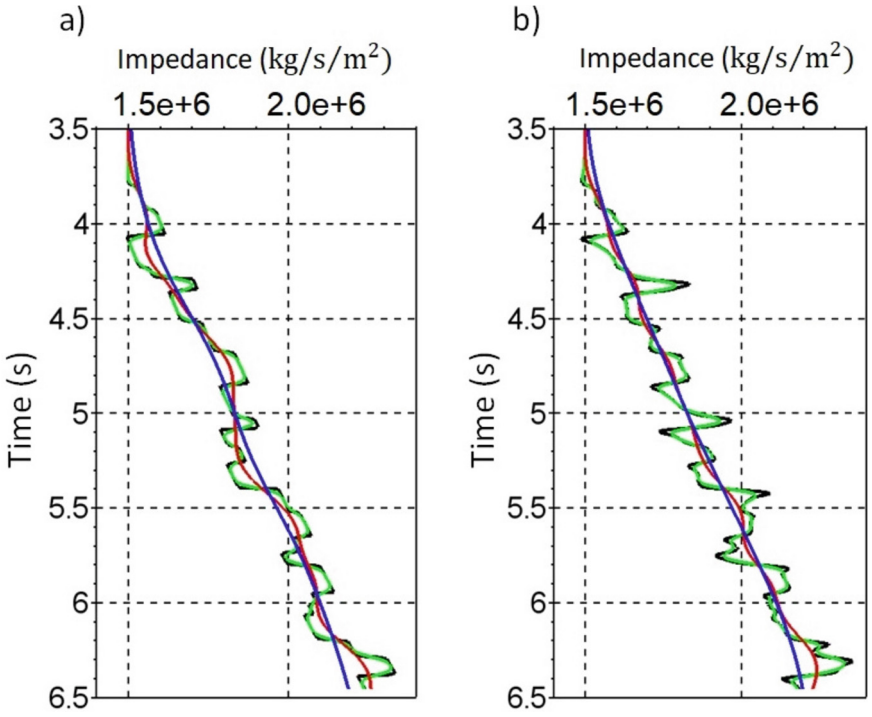

Fig. 6. a) The original model - black, and its smooth components at x = 6705 m: smoothing parameter b = 0.05 - green, b = 0.3 - red, b = 0.8 - blue; b) model obtained by inversion after migration - black, and its smooth components at x = 6705 m: smoothing parameter b = 0.05 - green, b = 0.3 - red, b = 0.8 - blue. (Color figure online)

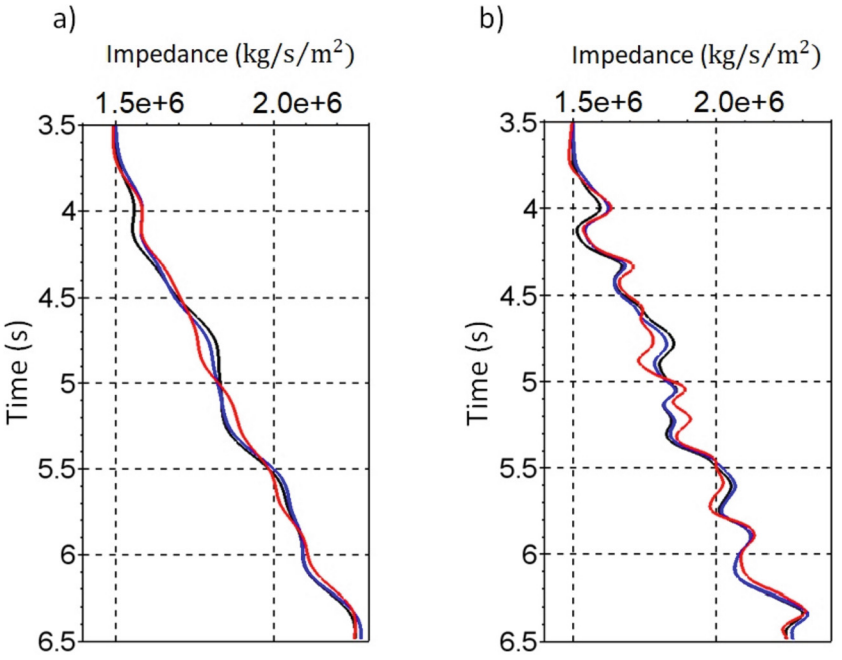

Fig. 7. Low-frequency components of models obtained by smoothing at x = 6705 m: a) parameter b = 0.3; b) b = 0.1. The smooth component of the true acoustic impedances is black, the result of the inversion of the ideal seismic trace is blue, the result of the inversion of the seismic trace after migration is red. (Color figure online)

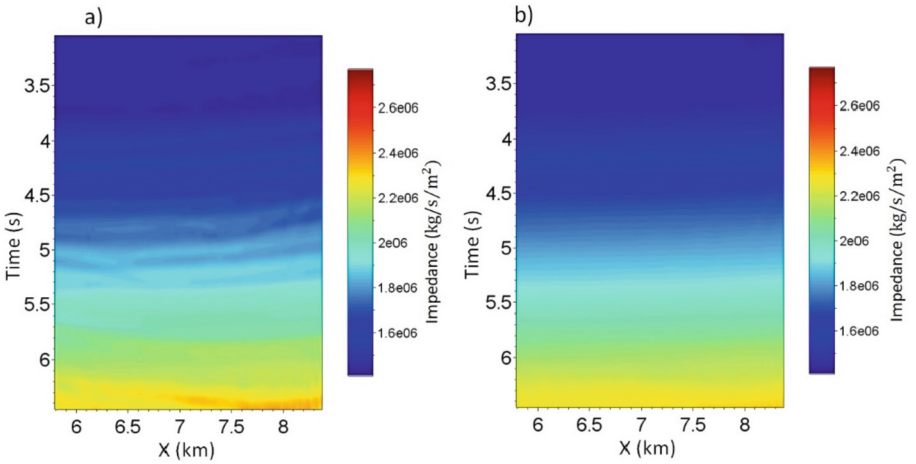

Fig. 8. Low-frequency components of the seismic inversion result after depth migration, obtained by smoothing with the parameter: a) b = 0.1; b) b = 0.3.

5 Conclusions

The paper presents an algorithm of seismic inversion after depth migration. It provides a study of the influence of the regularization parameter on the result of the inversion, as well as the influence of the regularization method itself. We extract low-frequency components from the impedance model and inversion results of ideal seismic traces and seismic traces after migration. We show model based seismic inversion of the depth seismic migration result reconstructs the high-frequency component of the model with acceptable quality. It is consistent with the standard application of seismic inversion to time processing results. By comparative analysis of the low-frequency components of the original model and the results of the inversion, we show that seismic inversion can recover the smooth component of the model. Such circumstances create prerequisites for using seismic inversion as a tool for refining the depth migration model.

Acknowledgments. The reported study was funded by RFBR and GACR, project number 20–55-26003.

References

1. Russell, B.H.: Introduction to Seismic Inversion Methods. Course Notes Series, pp. 80–101. Society of Exploration Geophysicists, Houston (1988)
2. Ampilov, Y., Barkov, A., Yakovlev, I.V., Filippova, K.E., Priezzhev, I.I.: Almost everything is about seismic inversion. Part 1. Seism. Technol. **4**, 3–16 (2009)
3. Russell, B.H., Hampson, D.P.: Comparison of poststack seismic inversion methods. In: SEG Technical Program Expanded Abstracts, pp. 876–878 (1991)
4. Hampson, D.P., Russell, B.H., Bankhead, B.: Simultaneous inversion of pre-stack seismic data. In: SEG Technical Program Expanded Abstracts, pp. 1633–1637 (2005)
5. Fletcher, R., Archer, S., Nichols, D., Mao, W.: Inversion after depth imaging. In: SEG Technical Program Expanded Abstracts, pp. 1–5 (2012)
6. Yakovlev, I.V., Ampilov, Y., Filippova, K.E.: Almost everything is about seismic inversion. Part 2. Seism. Technol. **1**, 5–15 (2011)
7. Li, Ts.: Development of noise-immune algorithms for dynamic inversion of seismic data. Ph.D. thesis (2017)
8. Tikhonov, A.N.: On ill-posed problems in linear algebra and a stable method for their solution. DAN SSSR **163**, 591–594 (1965)
9. Tikhonov, A.N., Arsenin, V.: Methods for Solving Ill-Posed Problems. Nauka, Moscow (1986)
10. Morozov, V.A.: On the regularization of ill-posed problems and the choice of the regularization parameter. J. Comput. Math. Math. Phys. **6**, 170–175 (1966)
11. Zhdanov, M.S.: Theory of Inverse Problems and Regularization in Geophysics. Nauchnyy Mir, Moscow (2007)
12. Protasov, M.I., Tcheverda, V.A.: True amplitude imaging. Dokl. Earth Sci. **407**, 441–445 (2006)
13. Protasov, M., Tcheverda, V.: True amplitude imaging by inverse generalized Radon transform based on Gaussian beam decomposition of the acoustic Green's function. Geophys. Prospect. **59**, 197–209 (2011)
14. Robein, E.: Seismic Imaging. EAGE Publications, Houten (2010)